



Rapid fabrication and improved electrical properties of $\text{CaCu}_3\text{Ti}_4\text{O}_{12}$ ceramics by sol–gel and spark plasma sintering techniques

Pu Mao¹ · Jiping Wang¹ · Lixue Zhang¹ · Shujuan Liu¹ · Yingying Zhao¹ · Qinzha Sun¹

Received: 20 March 2019 / Accepted: 17 June 2019 / Published online: 26 June 2019
© Springer Science+Business Media, LLC, part of Springer Nature 2019

Abstract

$\text{CaCu}_3\text{Ti}_4\text{O}_{12}$ (CCTO) ceramics with smaller grain size usually show a low dielectric constant by using the conventional sintering method. In this work, the pure CCTO ceramics with smaller grain size prepared by the spark plasma sintering method (SPS) present the giant dielectric constant (ϵ') over a wide temperature range. The dense CCTO ceramics have been rapidly fabricated by a sol–gel process and the SPS method at different sintering temperatures. The XRD patterns indicate a single CCTO phase with cubic perovskite structure in SPS-CCTO ceramics. The SEM images demonstrate that the average grain size of the SPS-CCTO ceramics increases from about $2.23(\pm 1.56)$ μm to $4.68(\pm 2.45)$ μm with the increases of the SPS sintering temperature from 800 to 900 °C. The obvious electrically heterogeneous characteristics in these SPS-CCTO ceramics are affirmed by the complex impedance spectroscopy analysis. The highest dielectric constant of 1.58×10^4 at 10^3 Hz is found in SPS-CCTO3 (900 °C) ceramics, and the temperature coefficients of the dielectric constant $\Delta\epsilon'$ in SPS-CCTO1 (800 °C) and SPS-CCTO2 (850 °C) ceramics with the high ϵ' values are less than $\pm 15\%$ ($\Delta\epsilon' < \pm 15\%$) over a temperature range of -30 to 80 °C; the high dielectric constant is due to the phenomenon of $R_g \ll R_{gb}$ based on the internal barrier layer capacitance (IBLC) effect. The larger nonlinear coefficient of 9.07, as well as the enhanced breakdown field of 3257 V/cm are achieved in SPS-CCTO1 ceramics, which is attributed to the increased grain boundary resistance and the Schottky barrier at grain boundary regions. These results indicate that the SPS method is an effective way to control the grain size and improve the electrical properties of the CCTO ceramics for energy storage application.

1 Introduction

Since the unusual cubic perovskite-related crystal structure and Pb-free dielectric materials, $\text{CaCu}_3\text{Ti}_4\text{O}_{12}$ (CCTO) ceramics, was reported by Subramanian et al. in 2000 [1], this material has attracted considerable attention recently and been much intensively investigated in detail due to its extraordinarily giant dielectric constant about 10^4 – 10^5 at room temperature and excellent nonlinear current density–electric field (J – E) characteristics without any doping [2–6]. Moreover, compared with the BaTiO_3 -based ceramics, the dielectric constant of the CCTO ceramics exhibit a good temperature stability over a wide range from 100 to

600 K without any structural or ferroelectric transition, and a weak frequency dependence in a range of 10^2 – 10^6 Hz [7, 8]. Owing to its remarkable electrical properties, the CCTO ceramics is very promising materials for the practical application in high-k capacitors, magnetic resonance imaging, microelectronics communication, microwave and energy storage devices [9–12].

For the giant dielectric behavior of the CCTO ceramics, despite many models from the intrinsic and extrinsic mechanism have proposed by many researchers, there is still doubt on its origin. So far, the internal barrier layer capacitor (IBLC) model, the extrinsic in nature, is widely accepted as the origin of the giant dielectric constant for CCTO ceramics. According to the IBLC model, there are many bulk grains with n-type semi-conductive behavior and grain boundaries with high resistance in CCTO ceramics, and the IBLC effect from the extrinsic polarization at the grain boundaries can responsible for the giant dielectric response [10, 13]. In addition, because of the charge trapping at the acceptor states, the Schottky barrier layers are created at interface between the n-type semiconducting grains, which

✉ Jiping Wang
jpwang@mail.xjtu.edu.cn

✉ Lixue Zhang
lxzhang@mail.xjtu.edu.cn

¹ State Key Laboratory for Mechanical Behavior of Materials, School of Materials Science and Engineering, Xi'an Jiaotong University, Xi'an 710049, China

also means that the back-to-back potential barriers formed by the band bending at the grain boundary regions [14]. And the Schottky potential barrier layers are responsible for the nonlinear J – E characteristics of the CCTO ceramics.

As known to all, the microstructure and electrostatic potential at grain boundary of the CCTO ceramics have a crucial effect on the electrical properties. Thus, the electrical performances can be enhanced effectively by the improved grain boundary response. In order to get the excellent electrical properties of the CCTO ceramics, many researchers have reported that the microstructure of ceramics is usually changed by using different fabrication methods (solid-state reaction, sol–gel et al.), and a conventional sintering (CS) process through optimizing the process parameters (the temperature and time of calcining and sintering) as well as changing the sintering atmosphere [15–18]. Moreover, a large number of studies show that the electrical performance of the CCTO ceramics have also improved by doping a variety of single elements and different pairs of elements [19], and mixing the other ceramics such as BaTiO₃ [20, 21], (Ba_{0.6}Sr_{0.4})TiO₃ [22], MgTiO₃ [23, 24], CaTiO₃ [23, 25], SrTiO₃ [23], TiO₂ [26]. However, for the traditional preparation method of the CCTO ceramics, the sintering temperature is higher and the sintering time is longer. The spark plasma sintering (SPS), as an electric field-assisted sintering technique (FAST) with rapid heating and short holding time in vacuum, can overcome the downsides of the conventional sintering method, which is a very rapid and efficient way to prepare electronic ceramics [27, 28]. At the same time, the mechanical strength of the SPS method for electronic ceramics can achieve the maximal values without adding the binder components which may contaminate the final products [29]. And the grain boundary layers can be strengthened by such method, which is beneficial to both the dielectric constant and nonlinear J – E characteristics. Ahmad et al. have utilized the mechanochemical synthesis and spark plasma sintering method to obtain the CCTO ceramics with two type-sized of micrometer (2–3 μm) and nanometer (80–200 nm), and the electrical and dielectric properties were studied by complex impedance spectroscopy and all the CCTO ceramics exhibited the giant dielectric constant [30, 31]. According to the study by Lin et al. the CCTO ceramics with different grain sizes (2–3 μm and 100–200 nm) were prepared by the solid-state reaction and SPS method, and their results indicate that the nonlinear J – E characteristics can be effectively tuned by facile sintering process control [32]. As mentioned above, the SPS method can obtain the smaller grain size than the conventional sintering process for CCTO ceramics, besides the electrically heterogeneous characteristics of the grain and grain boundary of the CCTO ceramics can be different during the short sintering period. Moreover, the temperature coefficient of the dielectric constant $\Delta\epsilon'$ in CCTO ceramics prepared by the SPS

method also should be considered for capacitor application. Therefore, it is an important and interesting work to research systematically the dielectric properties and its temperature stability, nonlinear J – E characteristics, complex impedance spectrum of the pure CCTO ceramics prepared by the SPS method for energy storage application.

In this study, we have successfully fabricated the pure phase CCTO ceramics with smaller grain size by a sol–gel and the spark plasma sintering techniques. The phase structure, microstructure, dielectric properties, temperature stability and nonlinear J – E characteristics of the SPS-CCTO ceramics were investigated in detail. Furthermore, from the grain boundary resistance and Schottky barrier height, the giant dielectric response mechanism and improved nonlinear J – E characteristics were also analyzed by the complex impedance spectroscopy.

2 Experimental procedures

2.1 Materials and method

The CCTO ceramics were prepared by the spark plasma sintering method. The CCTO precursor powders were synthesized by a sol–gel process, and the highly pure raw materials, Ca(NO₃)₂·4H₂O (99%, Alfa Aesar), Cu(NO₃)₂·3H₂O (99%, Alfa Aesar), Ti(C₃H₉O)₄, (99%, Alfa Aesar), were weight in precision according to the stoichiometric composition. Firstly, Ca(NO₃)₂·4H₂O and Cu(NO₃)₂·3H₂O were dissolved in anhydrous ethanol to form the homogeneous solution A, and citric acid was added into the solution A under magnetic stirring at room temperature. Meanwhile, Ti(C₃H₉O)₄ was dissolved in the anhydrous ethanol with magnetic stirring at room temperature to form the solution B. Secondly, the solution A was added into the solution B under continuous magnetic stirring at room temperature to obtain a clean and transparent sol solution. This sol solution was heated up to 90 °C to form a viscous blue gel, and then the gels were crushed and further heated to 120 °C for 12 h in the drying oven to obtain the fluffy precursor powders. Finally, the precursor powders were ground and calcined at 850 °C for 3 h to obtain the CCTO nanometer powders. Then, the CCTO powders were loaded into a cylindrical graphite die with a 12 mm inner diameter and sintered at various temperatures (heating rate: 100 °C/min) with holding time for 3 min under an axial pressure of 30 MPa provided by a SPS furnace (Ed-PASIII, Elenix Ltd, Japan), and followed by rapid cooling. Graphitic paper was wrapped around the CCTO nanometer powders for easy removal of the as-sintered samples. The SPS sintered CCTO ceramics with three different temperatures of 800 °C, 850 °C and 900 °C were labelled as SPS-CCTO1, SPS-CCTO2 and SPS-CCTO3, respectively. Prior to the characterization of the structure and

electrical properties, all samples were polished and treated with ultrasonic conditioning to remove the graphitic papers of their surface. And then all samples were thermally etched at 950 °C for 30 min in air atmosphere to clearly observe their grain and grain boundary structure.

2.2 Characterization methods

The phase structures of the CCTO powders and ceramics were identified by the X-ray diffraction (XRD, X Pert diffractometer, D8 Advance, Germany) with Cu K α radiation ($\lambda = 1.5406 \text{ \AA}$). The XRD data was recorded over the 2θ range of 10° – 90° at room temperature. Based on the XRD results, the lattice parameters were calculated to determine the changes in crystal structure of the CCTO ceramics. The densities of the samples were measured by the Archimedes method. Microstructures of the CCTO powders and ceramics were observed by a scanning electron microscope (SEM, Hitachi S-2700). The particle size of the CCTO powders and grain size of the CCTO ceramics were characterized by using the Nano Measure 1.2 Software from the SEM images. To measure the dielectric and nonlinear electrical properties, the CCTO ceramics surfaces were coated by the silver paste and then they were sintered at 800 °C for 30 min. The nonlinear DC current density–electric field intensity (J – E curves) characteristics were measured at room temperature by the high voltage measurement device (HP 34401A multimeter and WJ10001D precision linear high-voltage DC power). The frequency dependence of the dielectric properties and impedance of the CCTO ceramics were measured by the broadband dielectric spectrometer (Novolcontrol Concept 80, Germany) in a frequency range from 10^{-1} Hz to 10^7 Hz at a temperature range of -80 °C to 200 °C.

3 Results and discussion

3.1 Phase structure and composition

The XRD diffraction patterns of the calcined CCTO powders and SPS sintered ceramics are shown in Fig. 1a. All the primary diffraction peaks of the CCTO powders and ceramics are in keeping with the peaks of body centered cubic perovskite-related structure of the space group $Im\bar{3}$ according to the standard PDF database of the CCTO (JCPDF File No.75-2188), indicating that the CCTO phase has been formed in these samples. And the second phases of CuO and TiO₂ are detected in XRD pattern of the CCTO powders. Apparently, the impurity phase of CuO and TiO₂ have disappeared after the SPS sintering, and all ceramics show a cubic structure of the pure CCTO phase. Figure 1b shows the zoomed diffraction (220) peaks for the SPS-CCTO ceramics. It is found that the 220 peaks of the SPS-CCTO2 and SPS-CCTO3 ceramics all shift toward a lower angle compared to the SPS-CCTO1 ceramics, indicating an increase in lattice constants. This may be due to the change of the SPS sintering temperature. The lattice constants of the SPS-CCTO ceramics are given in Table 1, and these parameters are comparable to the value of 7.3910 Å reported in previous literature [1].

Table 1 Lattice constant and relative density of SPS-CCTO ceramics

Samples	SPS-CCTO1	SPS-CCTO2	SPS-CCTO3
Lattice constant (Å)	7.3837	7.3860	7.3856
Relative density (%)	95.61	97.55	95.27

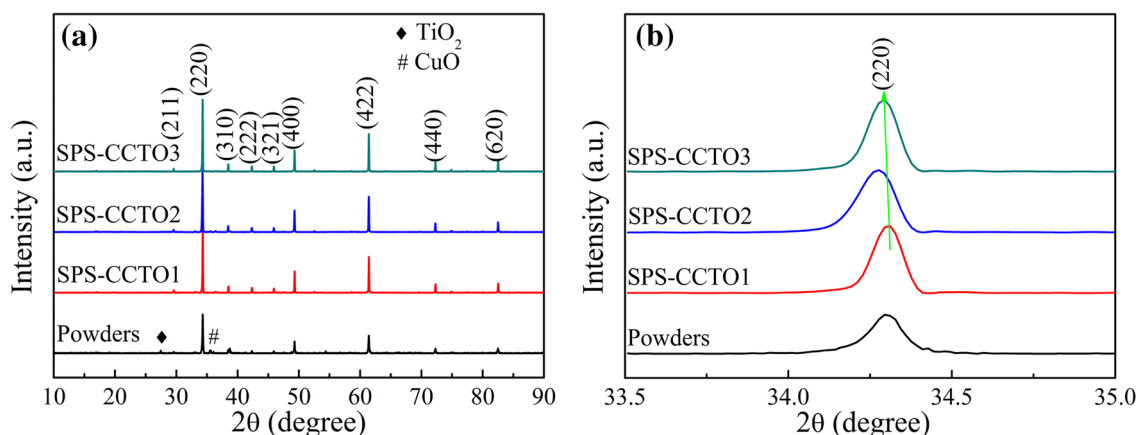


Fig. 1 XRD patterns (a), the zoomed XRD patterns of the peak (220) (b) of the calcined CCTO powders and SPS sintered CCTO ceramics (SPS-CCTO) with different SPS sintering temperatures

3.2 Microstructure characterization

The SEM images of the CCTO powders and SPS sintered ceramics are shown in Fig. 2. The mean particle size of the calcined CCTO powders is about $220.9(\pm 66.7)$ nm. All SPS-CCTO ceramics were polished and thermally etched to observe the internal evolution of the microstructure, and these SPS-CCTO ceramics exhibit an obvious grains and grain boundaries structure. The relative densities of the SPS-CCTO ceramics are summarized in Table 1. And the relative densities of all SPS-CCTO ceramics are more than 95.27%, which illustrate that the dense CCTO ceramics are successfully prepared by the SPS method in this work. Moreover, the CCTO ceramics with different SPS sintering temperature present the different grain sizes and its distributions, as shown in Fig. 3. It can be found that with the increase of the SPS sintering temperature from 800 to 900 °C, the average grain size of the SPS-CCTO

ceramics increase from $2.23(\pm 1.56)$ to $4.68(\pm 2.45)$ μm , which is smaller than the CCTO ceramics sintered by a conventional sintering process [33]. Generally, the perovskite phase is synthesized at the very high temperatures, and the grains have grown when the crystalline phase is fully formed. However, the plasma can be generated by the instantaneous discharge during the SPS sintering process, which enables each particle to generate uniform heat in the sintered body and enhance the activation energy at the surface of the particles. Therefore, the SPS sintered body can be densified in a relatively short time, and thus inhibiting the grains growth and obtaining the CCTO ceramics with smaller grain size [31, 32]. Meanwhile, the grain sizes of the SPS-CCTO ceramics all follow the Gaussian distribution, and the grain size distribution ranges become wider with the increase of the SPS sintering temperature. Therefore, the SPS sintering temperature play an important role to the grain size of the CCTO ceramics.

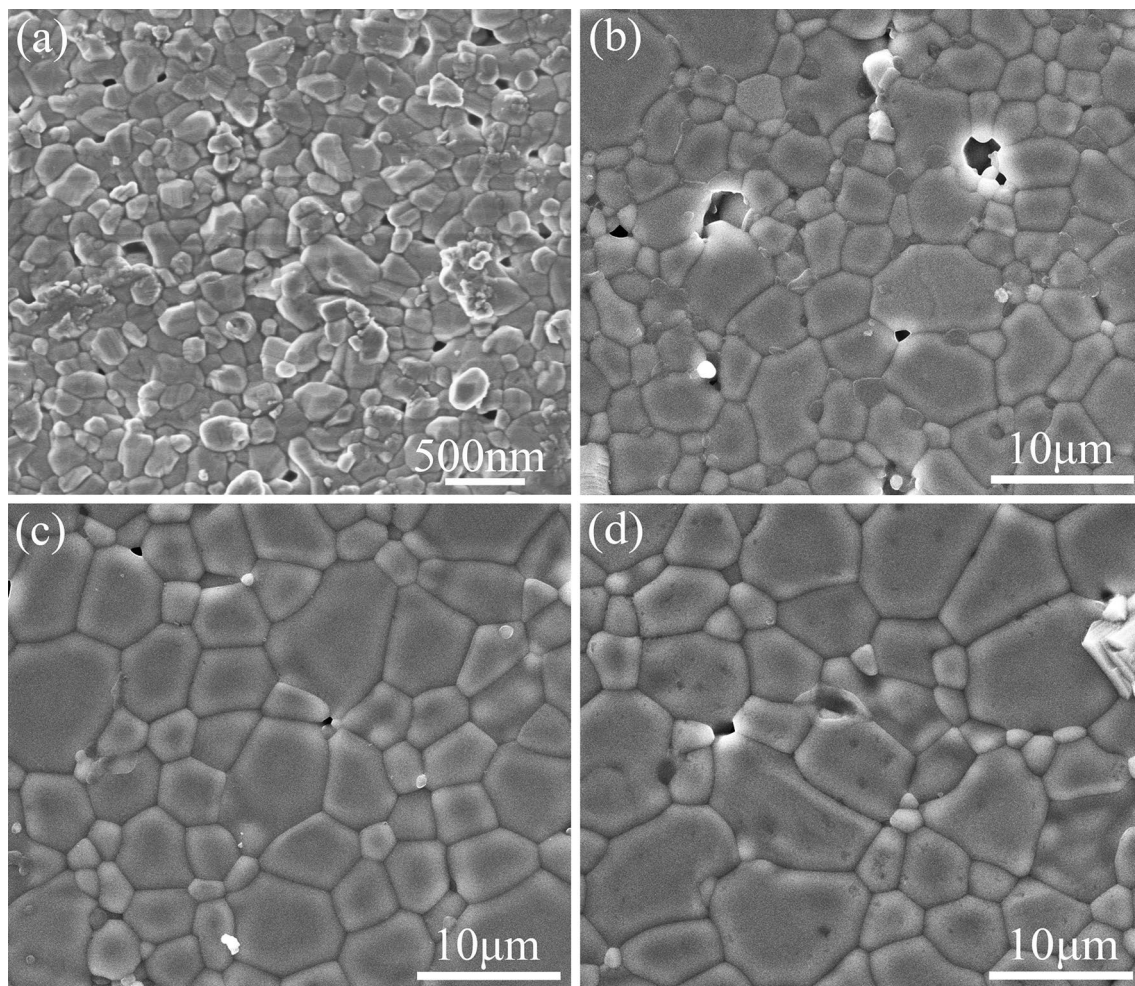


Fig. 2 SEM images of the calcined CCTO powders (a) and CCTO ceramics prepared by the SPS method: SPS-CCTO1 (b), SPS-CCTO2 (c), SPS-CCTO3 (d)

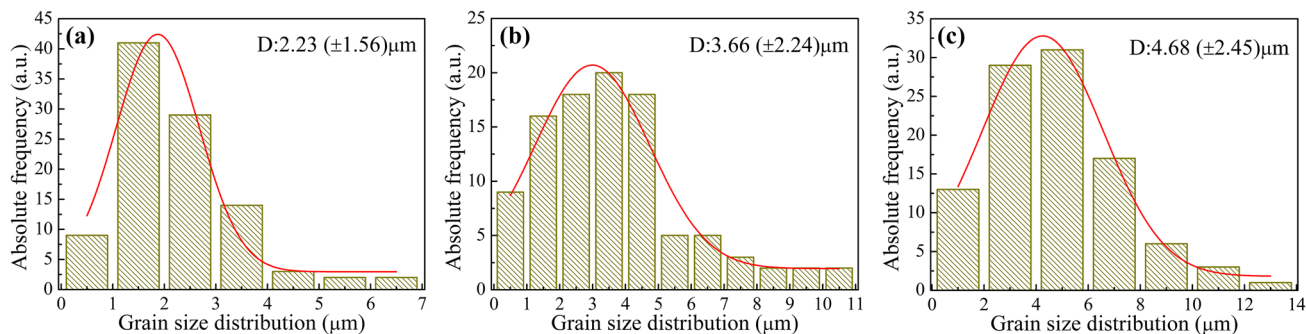


Fig. 3 The grain sizes and its distribution of the CCTO ceramics prepared by the SPS method: SPS-CCTO1 (a), SPS-CCTO2 (b), SPS-CCTO3 (c)

3.3 Dielectric properties

The frequency dependence of the relative dielectric constant (ϵ') and dielectric loss ($\tan\delta$) of the SPS-CCTO ceramics at room temperature is given in Fig. 4. These SPS-CCTO ceramics show the giant dielectric constant of 10^4 – 10^5 in this work, which is higher than the CCTO ceramics prepared by the conventional sintering process under the same grade of the average grain sizes compared to our previous work [34]. It can be found from Fig. 4a that the ϵ' values of the SPS-CCTO ceramics all decrease with the increase of frequency. The high ϵ' values of the SPS-CCTO ceramics are about 4.81×10^4 – 2.86×10^5 at low frequency (10^{-1} – 10 Hz). And the space charge polarization and electrode effect are suggested as a possible reason for the increased ϵ' values at low frequency [35]. At the intermediate frequency of 10 – 10^6 Hz, it is noticed that the ϵ' values of all SPS-CCTO ceramics increase with the SPS sintering temperature increasing. And the SPS-CCTO3 ceramics show the largest ϵ' value about 1.58×10^4 at a frequency of 10^3 Hz, which are comparable to the value of 2.14×10^4 for the SPS sintered CCTO ceramics

according to the previous reports [31]. This giant dielectric constant may be attributed to the electrically heterogeneous nature of the CCTO ceramics from the IBLC effects, such as the presence of the semiconducting grains and insulating grain boundaries. Furthermore, the effective dielectric constant (ϵ_{eff}) generally depends on the microstructure of the ceramic material and can be expressed as [31, 36]:

$$\epsilon_{eff} = \epsilon_{gb} \left(t_g / t_{gb} \right) \tag{1}$$

where ϵ_{gb} is the dielectric constant of the grain boundary, t_g and t_{gb} are the average grain size and the average thickness of the grain boundary layer, respectively. Based on the above equation, the effective dielectric constant is associated with the average grain size and the average thickness of the grain boundary layer, and the increase of the ϵ' value is major attributed to the increase of the average grain size. Therefore, the SPS-CCTO3 ceramics with larger average grain size exhibit the higher dielectric constant. And we can conclude that the larger grain size is beneficial to the higher dielectric constant, which is consistent with the

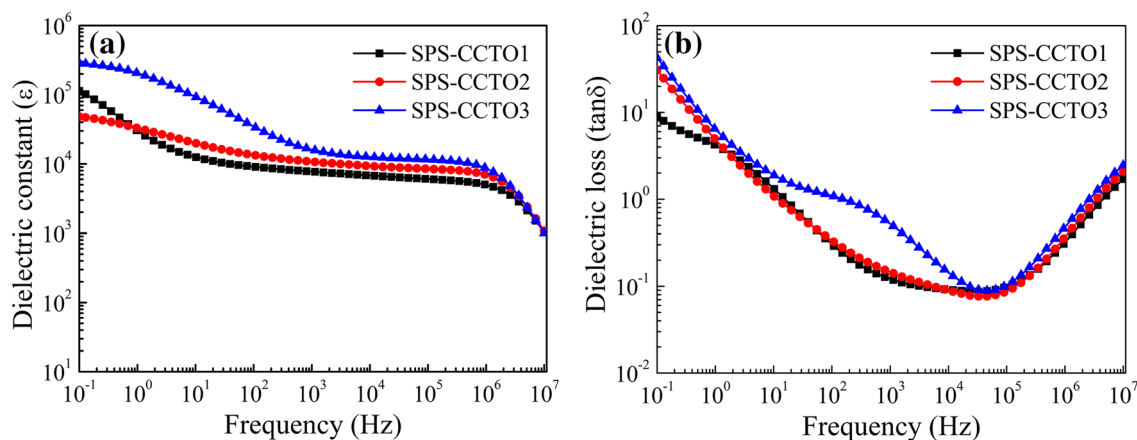


Fig. 4 The frequency dependence of the dielectric constant ϵ' (a) and dielectric loss $\tan\delta$ (b) at room temperature for SPS-CCTO ceramics

previous literature [37]. On the other hand, each dielectric constant curves show a stable plateau in a broad frequency range (10^2 – 10^6 Hz). Nevertheless, the ϵ' values of all SPS-CCTO ceramics display a sharply decreasing tendency at high frequency (10^6 – 10^7 Hz). It is considered that this may be related to the intrinsic grain relaxation. As shown in Fig. 4b, as the frequency increasing, the dielectric loss of all SPS-CCTO ceramics firstly decrease and followed a increase. It is possible that the electrode interface polarization or the dc conduction effect at low frequency and the Debye relaxation at high frequency contribute to the dielectric loss, respectively [13, 35]. Moreover, the SPS-CCTO1 ceramics exhibit a lower dielectric loss of 0.119 at 10^3 Hz, which is related to the more insulating grain boundary layers induced by the smaller average grain size.

The temperature dependence of the dielectric constant and dielectric loss of the SPS-CCTO ceramics at a frequency of 10^3 Hz is shown in Fig. 5a, b. It is clearly observed from Fig. 5a that the dielectric constant of the SPS-CCTO ceramics increase slowly with the increase of temperature over the range from -80 to 150 °C. And then the dielectric constants increase obviously when the test temperature exceed 150 °C, which may be attributed to the space charge polarization when the charge carrier accumulates at the interface between the samples and electrode [38, 39]. As demonstrated in Fig. 5b, the dielectric loss of the SPS-CCTO ceramics increase continually with the increase of test temperature. In general, the dielectric responses of the SPS-CCTO ceramics at high temperature is related to the dc conduction [35]. For the practical application in electronic devices, the temperature coefficient of the dielectric constant $\Delta\epsilon'$ is one of the important parameters besides the giant dielectric constant and low dielectric loss. Especially, the relevant standards specification of $\Delta\epsilon'$ should be less than $\pm 15\%$ ($\Delta\epsilon' < \pm 15\%$) for EIA code X5R, X7R, X8R and X9R capacitors are defined at the temperature ranges of -55 to 85 °C, -55 to 125 °C, -55 to 150 °C and -55 to 200 °C, respectively. The $\Delta\epsilon'$ can be evaluated at a frequency of 10^3 Hz by the following equation [40]:

$$\Delta\epsilon' = 100 \times \frac{\epsilon'_T - \epsilon'_{30}}{\epsilon'_{30}} (\%) \quad (2)$$

where ϵ'_T and ϵ'_{30} are the values of ϵ at a temperature of T and 30 °C, respectively. The $\Delta\epsilon'$ values at 10^3 Hz as a function of temperature for SPS-CCTO ceramics are shown in Fig. 5c. It is noteworthy that the $\Delta\epsilon'$ values of the SPS-CCTO1 and SPS-CCTO2 ceramics are lower than 15% over a temperature range of -30 to 80 °C, which indicates that these ceramics possess a better temperature stability than the SPS-CCTO3 ceramics.

3.4 Nonlinear current density–electric field (J – E) characteristics

The nonlinear current density–electric field (J – E) characteristics of the SPS-CCTO ceramics with different average grain sizes at room temperature are shown in Fig. 6. It can be found from Fig. 6a that all SPS-CCTO ceramics present a clearly nonlinear relationship between the current density and electric field. The breakdown field E_b value was obtained when the current density is $J = 1$ mA/cm². The nonlinear coefficient (α) was calculated by the formula as follows [41]:

$$\alpha = \frac{\log(J_2/J_1)}{\log(E_2/E_1)} \quad (3)$$

where E_1 and E_2 are the electric fields corresponding to $J_1 = 1$ mA/cm² and $J_1 = 10$ mA/cm², respectively. As shown in Fig. 6b, the breakdown field E_b values of the SPS-CCTO1, SPS-CCTO2 and SPS-CCTO3 ceramics are about 3256.59, 2418.70 and 621.88 V/cm, respectively. Apparently, the SPS-CCTO1 ceramics exhibit the highest breakdown field, which may be related to the more grain boundaries resulted from the smaller average grain size. On the one hand, the breakdown path of the SPS-CCTO ceramics with smaller grain size will pass across more grain boundaries and consume more energy in the dielectric breakdown process [42].

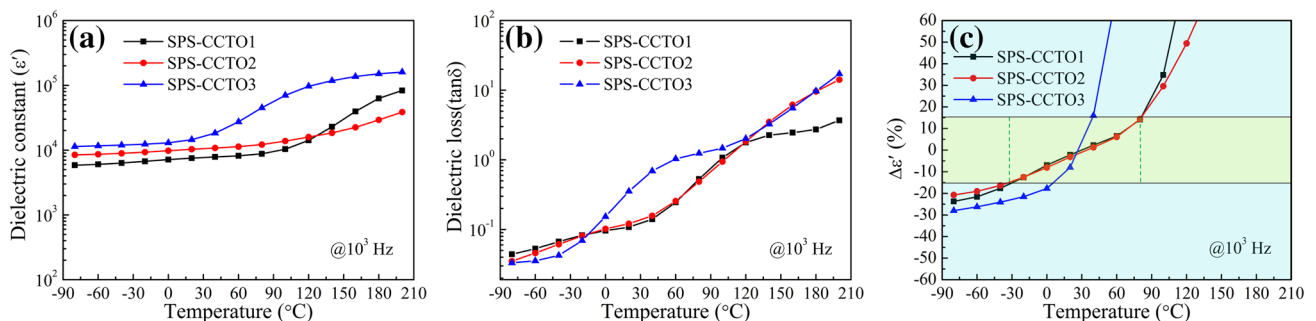


Fig. 5 The temperature dependence of the dielectric constant ϵ' (a), dielectric loss $\tan\delta$ (b) and the temperature coefficient of the dielectric constant $\Delta\epsilon'$ (c) at a frequency of 10^3 Hz over a temperature range of -80 to 200 °C for SPS-CCTO ceramics

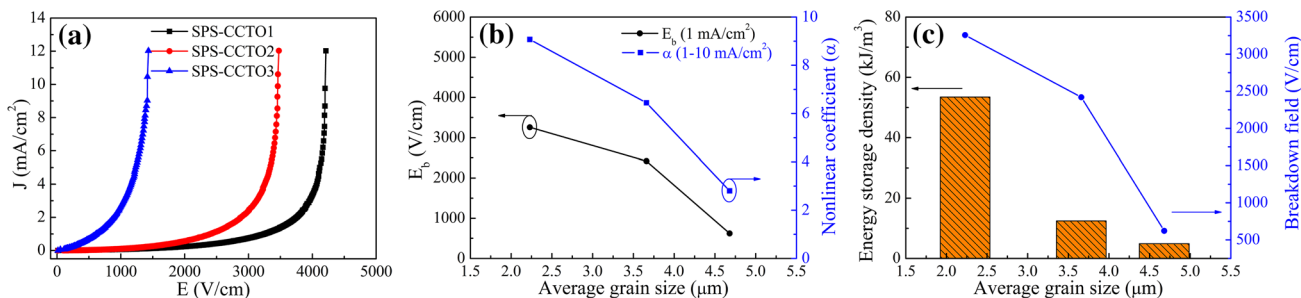


Fig. 6 Nonlinear $J-E$ characteristics (a), the breakdown field strength E_b and nonlinear coefficient α (b) and the energy storage density (c) of the SPS-CCTO1 (the average grain size of 2.23 μm), SPS-CCTO2

(the average grain size of 3.66 μm) and SPS-CCTO3 (the average grain size of 4.68 μm) ceramics

On the other hand, the dependence of the breakdown voltage on the grain size implies that internal interfaces such as grain boundary layers act as electrical potential barriers [3]. The breakdown voltage (V_s) can be determined in light of the following equation [43]:

$$V_s = \bar{N}\nu_b \tag{4}$$

where \bar{N} is the average number of the barrier, ν_b is the barrier voltage at the grain boundary. It can be seen that the breakdown voltage is roughly proportional to the average barrier number in series. As we all know, the average number of the barrier is inversely proportional to the average grain size. So, the breakdown voltage increases significantly with the decrease of the average grain size for CCTO ceramics, and it is easily understood that the SPS-CCTO1 ceramics with the smaller average grain size possesses the higher breakdown field. A similar phenomenon of the grain size effect on the breakdown field is found in the previous literature and our reported work [34, 37]. In addition, the nonlinear coefficient values α of the SPS-CCTO1, SPS-CCTO2 and SPS-CCTO3 ceramics have been obtained in the current density range of 1–10 mA/cm², which are 9.07, 6.44 and 2.80, respectively. It is noteworthy that the largest α value of 9.07 is relatively higher than the previously reported pure and doped CCTO ceramics [44–47]. Consequently, we claim that the changes of the grain size and grain boundary are crucial for the nonlinear $J-E$ characteristics of the CCTO ceramics, and this nonlinear behavior can be improved through optimizing the SPS fabrication process parameters, such as the sintering temperature, holding time, heating and cooling rate.

For energy storage devices, the high dielectric constant, breakdown field, energy storage density, frequency and temperature dependence are important parameters [48]. In particular, the breakdown field (E_b) plays a crucial role to the energy storage density of the dielectrics according to the following formula [49]:

$$U = \frac{1}{2}\epsilon_0\epsilon_r E_b^2 \tag{5}$$

where ϵ_0 is the vacuum permittivity (8.85×10^{-12} F/m), and ϵ_r is the relative permittivity. Based on the results of the dielectric constant and breakdown field, the energy storage densities at room temperature of the SPS-CCTO ceramics with different average grain sizes were calculated, as shown in Fig. 6c. The ϵ_r value of the maximum energy storage density is obtained from the ϵ' value at a frequency of 10^{-1} Hz. The Fig. 6c suggests that the highest energy storage density of 53.50 kJ/m³ with the highest breakdown field of 3256.59 V/cm is found in SPS-CCTO1 ceramics, which is over 10 times higher than the SPS-CCTO3 ceramics (about 4.89 kJ/m³ at 621.88 V/cm), and also higher than the reported literature [50]. In addition, we can notice that the variation tendency of the energy storage density is consistent with the breakdown field of the SPS-CCTO ceramics. Apparently, the promotion of the electrical properties can effectively enhance the energy storage density of the CCTO ceramics.

3.5 Complex impedance spectroscopy analysis

The complex impedance spectroscopy was performed to further investigate the effect of the fabrication parameters and microstructure changes on the electrically heterogeneous grain/grain boundary characteristics of the SPS-CCTO ceramics. According to the IBL model, an equivalent circuit with two parallel resistance and capacitance (RC) elements in series can explain the electrical heterogeneity of the semiconducting grains and insulating grain boundaries. The complex impedance Z^* can be calculated as the following formula [51]:

$$Z^* = Z' - iZ'' = \frac{R_{gb}}{1 + i\omega R_{gb}C_{gb}} + \frac{R_g}{1 + i\omega R_g C_g} \tag{6}$$

$$Z' = \frac{R_g}{1 + (\omega R_g C_g)^2} + \frac{R_{gb}}{1 + (\omega R_{gb} C_{gb})^2} \tag{7}$$

$$Z'' = R_g \left[\frac{\omega R_g C_g}{1 + (\omega R_g C_g)^2} \right] + R_{gb} \left[\frac{\omega R_{gb} C_{gb}}{1 + (\omega R_{gb} C_{gb})^2} \right] \quad (8)$$

where Z' is the real part and Z'' is the imaginary part of complex impedance Z^* , R_g and C_g , in one RC element, represent the resistance and capacitance of the semiconducting grains, while R_{gb} and C_{gb} are the resistance and capacitance of the insulating grain boundaries in another RC element. The impedance measurement data were fitted based on the corresponding equivalent circuits by using the software ZView2, and then the values of R_g and R_{gb} can be obtained at high and low frequencies, respectively. The Cole–Cole impedance plots of the SPS-CCTO ceramics with different average grain sizes at room temperature are shown in Fig. 7a–c. The R_g and R_{gb} values dependence on average grain sizes of the SPS-CCTO ceramics are given in Fig. 7d, e. It can be seen that the R_g values of the SPS-CCTO ceramics are about 6.58–8.84 Ω , thus confirming the semiconducting nature of the grains. And these R_g values are far smaller than the R_{gb} values approximately 1.20×10^5 – 1.39×10^6 Ω , indicating the electrically heterogeneous characteristics of the semiconducting grain and insulating grain boundary. The frequency dependence of the imaginary part Z'' of complex impedance Z^* at room temperature for SPS-CCTO ceramics is presented in Fig. 7f. The peak values of Z'' are proportional to the associated resistance. As shown in Fig. 7f, the SPS-CCTO1 ceramics exhibit the highest peak values of Z'' , and the Z''

peak shifts to the higher frequency than the SPS-CCTO2 and SPS-CCTO3 ceramics. Furthermore, the grain boundary responses with the Z'' peak values at low frequency are much larger than the grain responses at high frequency, which is $R_g \ll R_{gb}$. Since the phenomenon of $R_g \ll R_{gb}$, the obvious electrical heterogeneity exists in SPS-CCTO ceramics. In order to compare the grain size effect on electrically heterogeneous and dielectric properties, the comparison of the ϵ' , $\tan \delta$, R_g and R_{gb} values of the SPS-CCTO ceramics in this work with the CCTO ceramics prepared by the conventional sintering (CS) method or SPS technique in other researches and our reported work are summarized in Table 2. It can be seen that the electrically heterogeneous characteristics of the SPS-CCTO ceramics in this work is comparable with the CCTO ceramics prepared by the CS process and SPS method under the same grade of the grain sizes [31, 34, 40], while the R_g value is lower, which may be responsible for the giant dielectric behavior in SPS-CCTO ceramics. In addition, the R_g and R_{gb} values decrease with the increase of the average grain size corresponding to the SPS-CCTO1, SPS-CCTO2, SPS-CCTO3 ceramics, respectively. This indicated that the grain sizes under the SPS sintering temperature have an important influence on the resistance of the grain and grain boundary for CCTO ceramics. And the SPS-CCTO1 ceramics with the smaller grain size possesses the higher R_{gb} value, which may be attributed to the more grain boundary layers. According to the IBLC model, with the decrease of the average grain size, the number of the

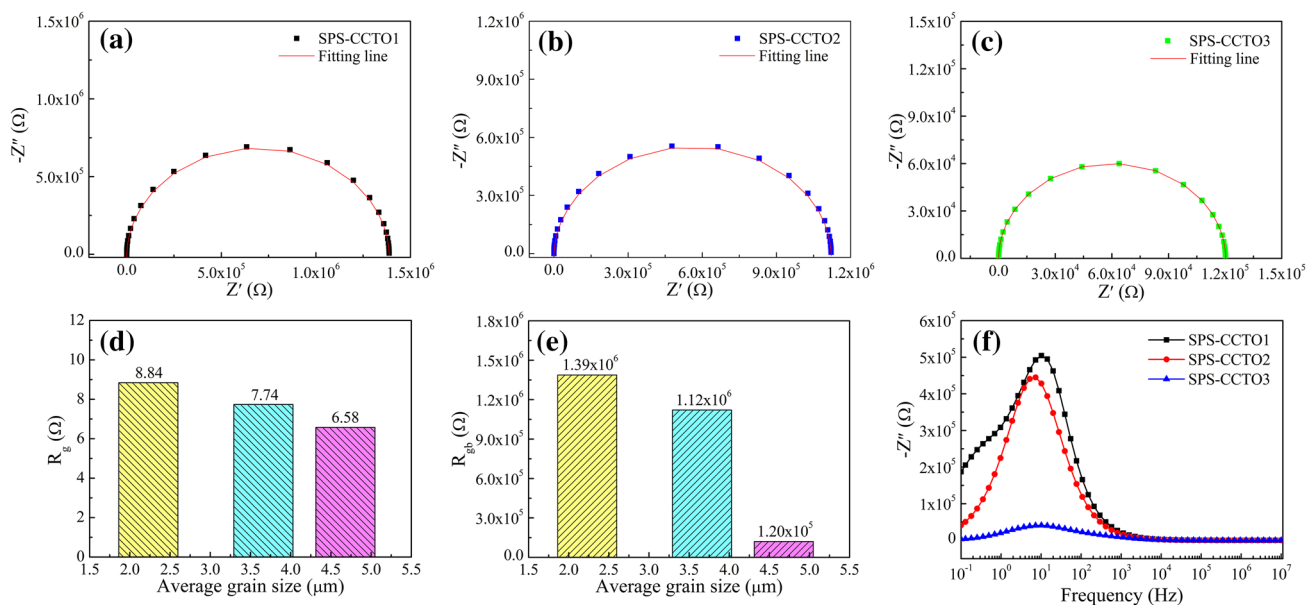


Fig. 7 The impedance complex plane plots at room temperature (a–c), the grain resistance R_g (d), grain boundary R_{gb} (e) and frequency dependence of Z'' at room temperature (f) of the SPS-CCTO1 (the

average grain size of 2.23 μm), SPS-CCTO2 (the average grain size of 3.66 μm) and SPS-CCTO3 (the average grain size of 4.68 μm) ceramics

Table 2 Comparison of the ϵ' , $\tan\delta$, R_g and R_{gb} values of the SPS-CCTO ceramics prepared by the SPS method in this work with the CCTO ceramics prepared by the conventional sintering (CS) method or SPS technique in other researches and our reported work

Samples	Sintering process	Grain size	ϵ'	$\tan\delta$	R_g (Ω)	R_{gb} (Ω)	Ref.
CCTO1-8	CS	2.89(\pm 0.89) μm	9870	0.132	56	–	[40]
CCTO1	CS	2.03(\pm 0.66) μm	797	0.102	56.39	2.98×10^7	[34]
CCTO2	CS	2.96(\pm 0.84) μm	1341	0.104	43.17	1.80×10^7	[34]
CCTO3	CS	3.73(\pm 1.10) μm	2358	0.103	42.05	1.42×10^7	[34]
SPS-800	SPS	~ 80 nm	8.3×10^3	–	110	2.00×10^5	[31]
SPS-900	SPS	100–150 nm	2.4×10^4	–	60	3.06×10^4	[31]
SPS-975	SPS	150–200 nm	3.2×10^4	–	30	3.00×10^5	[31]
SPS-150	SPS	2–3 μm	2.14×10^4	–	61	1.35×10^4	[31]
SPS-CCTO1	SPS	2.23(\pm 1.56) μm	7.68×10^3	0.119	8.84	1.39×10^6	This work
SPS-CCTO2	SPS	3.66(\pm 2.24) μm	1.07×10^4	0.141	7.74	1.12×10^6	This work
SPS-CCTO3	SPS	4.68(\pm 2.45) μm	1.58×10^4	0.490	6.58	1.20×10^5	This work

insulating grain boundary layers increasing, leading to the higher grain boundary resistance of the CCTO ceramics.

Generally, the electrical response from the grain boundary is owed to the larger resistance and capacitance than that of the grain [52]. Due to the grain boundary response from the IBL model, the dielectric loss of the CCTO ceramics is mainly related to the R_{gb} value at low frequency [53]. It is noticed that the change trend of the R_{gb} values is consistent with the dielectric loss at low frequency of the SPS-CCTO ceramics, as shown in Fig. 4b. Whereas, the increase of the dielectric loss at high frequency is attributed to the high capacitance $C_p(\epsilon)$ of the CCTO ceramics. Moreover, the impedance spectroscopy can also explain the nonlinear J – E properties of the CCTO ceramics. The decreases of the grain size results in the R_{gb} value increasing, which can make contributions to the highest breakdown field of the CCTO ceramics with the largest R_{gb} value.

The electronic structure at grain boundary has an effect on dielectric and nonlinear properties of the SPS-CCTO ceramics. In particular, the formation of the Schottky barrier at grain boundary is associated with the nonlinear behavior of the CCTO ceramics. It is well known that the electrons transport under electric field follows the thermionic emission

model, which leads to the nonlinear J – E characteristics of the CCTO ceramics [54]. Moreover, the activation energy is associated with the potential energy barrier height, which restricts the motion of the charge carrier [55]. The activation energy of the grain (E_g) and grain boundary (E_{gb}) can be calculated by using the Arrhenius equation, as following:

$$\ln\sigma_{g,gb} = \left(\frac{-E_{g,gb}}{k_B T} \right) + \ln\sigma_0 \quad (9)$$

where σ_g and σ_{gb} are the electrical conductivity of the grain and grain boundary, expressed as $\sigma_g(\sigma_{gb}) = 1/R_g(R_{gb})$, σ_0 is the pre-exponential factor, k_B is Boltzmann constant and T is the absolute temperature. The $\ln(\sigma_g/\sigma_{gb})$ values show a good linear relationship with $1000/T$ for the SPS-CCTO ceramics in the fitted plots, as shown in Fig. 8a, b. The activation energy values of the grain and grain boundary of the CCTO ceramics can be obtained from the slopes of the fitted straight lines, as given in Fig. 8c. It can be seen in Fig. 8c that the E_g values are about 0.057, 0.062 and 0.067 eV, while the E_{gb} values are found to be 0.682, 0.610 and 0.555 eV for SPS-CCTO1, SPS-CCTO2 and SPS-CCTO3 ceramics, respectively. And the E_g values are lower than the E_{gb} values

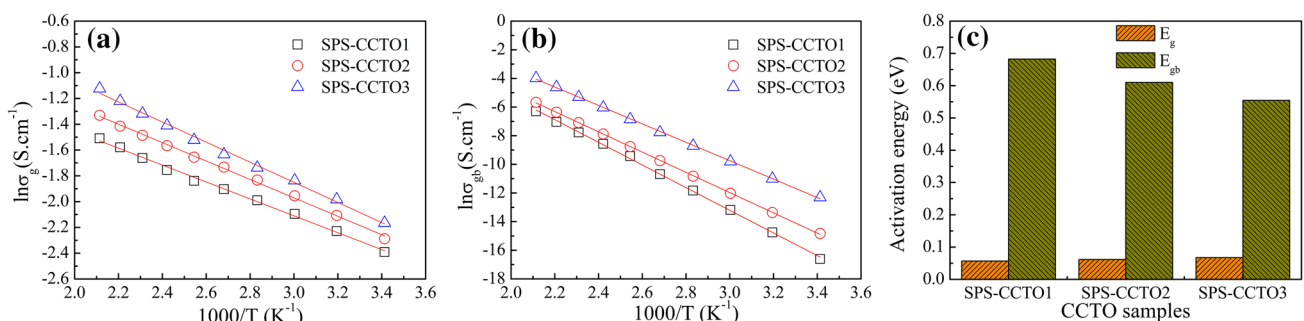


Fig. 8 Arrhenius plots of the $\ln\sigma_g$ (a) and $\ln\sigma_{gb}$ (b) versus $1000/T$; the activation energy of the grain (E_g) and grain boundary (E_{gb}) (c) for SPS-CCTO ceramics

of the SPS-CCTO ceramics, which is agreement with the previous reports [33]. However, the E_{gb} value of the SPS-CCTO1 ceramics is larger than the SPS-CCTO2 and SPS-CCTO3 ceramics, which is well corresponding to the higher grain boundary resistance and enhanced breakdown field. This indicates that the more grain boundary layers induced by the smaller grain size can change the electrically heterogeneous characteristics and improve the electrical properties of the SPS sintered CCTO ceramics. Furthermore, the higher E_{gb} value may imply that the motion of the charge carriers needs to overcome the higher Schottky barrier layers, which can contribute to the enhanced breakdown field and nonlinear coefficient.

4 Conclusion

In summary, the CCTO nanometer powders were successfully prepared by a sol–gel method, and the dense CCTO ceramics were rapidly fabricated via the SPS process with different sintering temperatures. The XRD analysis confirmed that all the SPS sintered ceramics showed the perovskite-type cubic structure of the pure CCTO phase. From the SEM image results, with the increase of the SPS temperature from 800 to 900 °C, the average grain sizes of the SPS-CCTO ceramics increase slightly from about $2.23(\pm 1.56)$ μm to $4.68(\pm 2.45)$ μm . The giant dielectric constants were obtained in SPS-CCTO ceramics, and the SPS-CCTO3 (900 °C) ceramics exhibit the highest dielectric constant about 1.58×10^4 at a frequency of 10^3 Hz. Meanwhile, the temperature coefficients of the dielectric constant in SPS-CCTO1 and SPS-CCTO2 ceramics are less than $\pm 15\%$ at a temperature range of -30 to 80 °C. The giant dielectric response of the CCTO ceramics is attributed to the electrical heterogeneity according to the IBLC model, which can be supported by the $R_g \ll R_{gb}$ phenomenon from the complex impedance spectrum. In addition, it is found that all the SPS-CCTO ceramics demonstrate the obvious nonlinear behavior, and the SPS-CCTO1 (800 °C) ceramics present the higher nonlinear coefficient of 9.07 as well as the higher breakdown field of 3256.59 V/cm than the others. The improved breakdown field through can be attributed to the increased grain boundary resistance, as well as the formed Schottky barrier at grain boundary regions, which is confirmed by the activation energy of the grain boundary. Therefore, using the SPS process is an effective and rapid method to prepare the CCTO ceramics with excellent electrical properties for energy storage application.

Acknowledgements This work was supported by the National Natural Science Foundation of China (Grant Nos. 51772242, 51621063), the Innovative Research Team of Ministry of Education of China (Grant

No. IRT13034) and the Fundamental Research Funds for the Central Universities (Grant No. xjj2016017).

References

1. M.A. Subramanian, D. Li, N. Duan, B.A. Reisner, A.W. Sleight, *J. Solid State Chem.* **151**, 323 (2000)
2. C.C. Homes, T. Vogt, S.M. Shapiro, S. Wakimoto, A.P. Ramirez, *Science* **293**, 673 (2001)
3. S.Y. Chung, I.L.D. Kim, S.J. Kang, *Nat. Mater.* **3**, 774 (2004)
4. S.Y. Chung, J.H. Choi, J.K. Choi, *Appl. Phys. Lett.* **91**, 091912 (2007)
5. L. Singh, B.C. Sin, I.W. Kim, K.D. Mandal, H. Chung, Y. Lee, *J. Am. Ceram. Soc.* **99**, 27 (2016)
6. J.A. Cortés, G. Cotrim, S. Orrego, A.Z. Simões, M.A. Ramírez, *J. Alloys Compd.* **735**, 140 (2018)
7. W. Si, E.M. Cruz, P.D. Johnson, P.W. Barnes, P. Woodward, A.P. Ramirez, *Appl. Phys. Lett.* **81**, 2056 (2002)
8. J. Sebald, S. Krohns, P. Lunkenheimer, S.G. Ebbinghaus, S. Riegg, A. Reller, A. Loidl, *Solid State Commun.* **150**, 857 (2010)
9. T.T. Fang, C.P. Liu, *Chem. Mater.* **17**, 5167 (2005)
10. R. Espinoza-González, E. Mosquera, *Ceram. Int.* **43**, 14659 (2017)
11. S. Rani, N. Ahlawat, K.M. Sangwan, S. Rani, R. Punia, J. Malik, *J. Mater. Sci.* **29**, 10825 (2018)
12. Y.P. Qu, Y. Du, G.H. Fan, J.H. Xin, Y. Liu, P.T. Xie, S.X. You, Z.D. Zhang, K. Sun, R.H. Fan, *J. Alloys Compd.* **771**, 699 (2019)
13. M.H. Cohen, J.B. Neaton, L.X. He, D. Vanderbilt, *J. Appl. Phys.* **94**, 3299 (2003)
14. N. Barman, K.B.R. Varma, *Ceram. Int.* **43**, 6363 (2017)
15. R. Yu, H. Xue, Z.L. Cao, L. Chen, Z.X. Xiong, *J. Eur. Ceram. Soc.* **32**, 1245 (2012)
16. R. Schmidt, M.C. Stennett, N.C. Hyatt, J. Pokorny, J. Prado-Gonjal, M. Li, D.C. Sinclair, *J. Eur. Ceram. Soc.* **32**, 3313 (2012)
17. P. Liu, Y.M. Lai, Y.M. Zeng, S. Wu, Z.H. Huang, J. Han, *J. Alloys Compd.* **650**, 59 (2015)
18. T. Li, R.Z. Xue, J.H. Hao, Y.C. Xue, Z.P. Chen, *J. Alloys Compd.* **509**, 1025 (2011)
19. M. Ahmadipour, M.F. Ain, Z.A. Ahmad, *Nano-Micro Lett.* **8**, 291 (2016)
20. L. Singh, U.S. Rai, K.D. Mandal, B.C. Sin, H.I. Lee, H. Chung, Y. Lee, *Mater. Charact.* **96**, 54 (2014)
21. H.E. Kim, S.M. Choi, Y.W. Hong, S.I. Yoo, *J. Alloys Compd.* **610**, 594 (2014)
22. I. Norezan, A.K. Yahya, M.K. Talari, *J. Mater. Sci. Technol.* **28**, 1137 (2012)
23. D. Xu, K. He, R.H. Yu, L. Jiao, H.M. Yuan, X.J. Sun, G.P. Zhao, H.X. Xu, X.N. Cheng, *J. Alloys Compd.* **592**, 220 (2014)
24. J.C. Yuan, Y.H. Lin, H.F. Lu, B. Cheng, C.W. Nan, *J. Am. Ceram. Soc.* **94**, 1966 (2011)
25. L. Ramajo, R. Parra, J.A. Varela, M.M. Reboledo, M.A. Ramírez, M.S. Castro, *J. Alloys Compd.* **497**, 349 (2010)
26. W.T. Hao, P.P. Xu, M.W. Wang, S. Yang, W. Yupeng, H. Wu, L. Sun, E.S. Cao, Y.J. Zhang, *J. Alloys Compd.* **740**, 1159 (2018)
27. P. Roy, V. Pal, T. Maiti, *Ceram. Int.* **43**, 12809 (2017)
28. L. Wang, X.Y. Shu, F.C. Yi, D.D. Shao, K.B. Zhang, H.B. Zhang, X.R. Lu, *J. Eur. Ceram. Soc.* **38**, 2863 (2018)
29. E.K. Papynov, O.O. Shichalin, E.B. Modin, V.Yu. Mayorov, A.S. Portnyagin, S.P. Kobylakov, A.V. Golub, M.A. Medkov, I.G. Tananaev, V.A. Avramenko, *RSC Adv.* **6**, 34066 (2016)
30. M.M. Ahmad, *Appl. Phys. Lett.* **102**, 232908 (2013)
31. M.M. Ahmad, K. Yamada, *J. Appl. Phys.* **115**, 154103 (2014)

32. H. Lin, X. He, Y.Y. Gong, D.F. Pang, Z.G. Yi, *Ceram. Int.* **44**, 8650 (2018)
33. D.L. Sun, A.Y. Wu, S.T. Yin, *J. Am. Ceram. Soc.* **91**, 169 (2007)
34. P. Mao, J.P. Wang, S.J. Liu, L.X. Zhang, Y.Y. Zhao, L.Q. He, *J. Alloys Compd.* **778**, 625 (2019)
35. K.N. Wu, Y.W. Huang, J.Y. Li, S.T. Li, *Appl. Phys. Lett.* **111**, 042902 (2017)
36. T.B. Adams, D.C. Sinclair, A.R. West, *Phys. Rev. B* **73**, 094124 (2006)
37. T. Li, Z.P. Chen, Y.L. Su, L. Su, J.C. Zhang, *J. Mater. Sci.* **44**, 6149 (2009)
38. A.K. Rai, K.D. Mandal, D. Kumar, O. Parkash, *J. Alloys Compd.* **491**, 507 (2010)
39. L. Ni, X.M. Chen, *Appl. Phys. Lett.* **91**, 122905 (2007)
40. K. Prompa, E. Swatsitang, T. Putjuso, *J. Mater. Sci.* **28**, 15033 (2017)
41. K. Prompa, E. Swatsitang, C. Saiyasombat, T. Putjuso, *Ceram. Int.* **44**, 13267 (2018)
42. Z.M. Cai, X.H. Wang, W. Hong, B.C. Luo, Q.C. Zhao, L.T. Li, *J. Am. Ceram. Soc.* **101**, 5487 (2018)
43. J.F. Wang, W.B. Su, H.C. Chen, W.X. Wang, G.Z. Zang, *J. Am. Ceram. Soc.* **88**, 331 (2005)
44. S. Rhouma, S. Saïd, C. Autret, S.D. Almeida-Didry, M.E. Amrani, A. Megriche, *J. Alloys Compd.* **717**, 121 (2017)
45. J. Wang, Z.Y. Lu, T.F. Deng, C.F. Zhong, Z.W. Chen, *J. Eur. Ceram. Soc.* **38**, 3505 (2018)
46. L. Sun, Q. Ni, J.Q. Guo, E.S. Cao, W.T. Hao, Y.J. Zhang, L. Ju, *Appl. Phys. A* **124**, 428 (2018)
47. J. Boonlakhorn, P. Kidkhunthod, N. Chanlek, P. Thongbai, *J. Eur. Ceram. Soc.* **38**, 137 (2018)
48. J.W. Lee, J.H. Koh, *Ceram. Int.* **43**, 9493 (2017)
49. Z.M. Dang, J.K. Yuan, S.H. Yao, R.J. Liao, *Adv. Mater.* **25**, 6334 (2013)
50. X.T. Zhao, L.L. Ren, L.J. Yang, S. Li, R.J. Liao, W.W. Li, J.Y. Li, *I.E.E.E. Trans., Dielectr. Electr. Insul.* **24**, 764 (2017)
51. D.C. Sinclair, T.B. Adams, F.D. Morrison, A.R. West, *Appl. Phys. Lett.* **80**, 2153 (2002)
52. D.C. Sinclair, A.R. West, *J. Appl. Phys.* **66**, 3850 (1989)
53. Z. Kafi, A. Kompany, H. Arabi, A. Khorsand Zak, *J. Alloys Compd.* **727**, 168 (2017)
54. J.Y. Li, X.T. Zhao, F. Gu, S.T. Li, *Appl. Phys. Lett.* **100**, 202905 (2012)
55. L.J. Liu, H.Q. Fan, P.Y. Fang, X.L. Chen, *MRS Bull.* **43**, 1800 (2008)

Publisher's Note Springer Nature remains neutral with regard to jurisdictional claims in published maps and institutional affiliations.